Can Polar Lows be Objectively Identified and Tracked in the ECMWF Operational Analysis and the ERA-Interim Reanalysis?

GIUSEPPE ZAPPA AND LEN SHAFFREY

National Centre for Atmospheric Science, Department of Meteorology, University of Reading, Reading, United Kingdom

KEVIN HODGES

National Centre for Earth Observation, University of Reading, Reading, United Kingdom

(Manuscript received 18 February 2014, in final form 2 April 2014)

ABSTRACT

Polar lows are maritime mesocyclones associated with intense surface wind speeds and oceanic heat fluxes at high latitudes. The ability of the Interim ECMWF Re-Analysis (ERA-Interim, hereafter ERAI) to represent polar lows in the North Atlantic is assessed by comparing ERAI and the ECMWF operational analysis for the period 2008–11. First, the representation of a set of satellite-observed polar lows over the Norwegian and Barents Seas in the operational analysis and ERAI is analyzed. Then, the possibility of directly identifying and tracking the polar lows in the operational analysis and ERAI is explored using a tracking algorithm based on 850-hPa vorticity with objective identification criteria on cyclone dynamical intensity and atmospheric static stability. All but one of the satellite-observed polar lows with a lifetime of at least 6 h have an 850-hPa vorticity signature of a collocated mesocyclone in both the operational analysis and ERAI for most of their life cycles. However, the operational analysis has vorticity structures that better resemble the observed cloud patterns and stronger surface wind speed intensities compared to those in ERAI. By applying the objective identification criteria, about 55% of the satellite-observed polar lows are identified and tracked in ERAI, while this fraction increases to about 70% in the operational analysis. Particularly in ERAI, the remaining observed polar lows are mainly not identified because they have too weak wind speed and vorticity intensity compared to the tested criteria. The implication of the tendency of ERAI to underestimate the polar low dynamical intensity for future studies of polar lows is discussed.

1. Introduction

Polar lows are intense maritime mesocyclones forming at high latitudes during cold air outbreaks (Rasmussen and Turner 2003). They have a radius of the order of 100–500 km and surface wind speeds above 15 m s^{-1}. This makes them a major source of weather risk in high-latitude coastal areas and it raises interest in how they might be affected by climate change (Kolstad and Bracegirdle 2008; Zahn and von Storch 2010). Moreover, polar lows are associated with large heat fluxes out of the ocean (Shapiro et al. 1987) that in regions subject to deep-water formation, such as the Greenland, Norwegian, and Irminger Seas, can destabilize the water column and affect the Atlantic meridional overturning circulation (Condron et al. 2008; Condron and Renfrew 2013; Bourassa et al. 2013). Therefore, there are multiple reasons for understanding how well atmospheric reanalyses and climate models can represent polar lows.

Polar lows have been initially detected by the inspection of weather maps and weather station data (Wilhelmsen 1985) and later identified from their characteristic spiraliform or comma-shaped cloud patterns in satellite images (Businger 1985; Blechschmidt 2008; Noer et al. 2011). More recently, polar lows have also been directly identified and tracked in the numerical weather prediction and regional climate models output using objective identification criteria (Bracegirdle and Gray 2008; Zahn and

Denotes Open Access content.

Corresponding author address: Giuseppe Zappa, Department of Meteorology, University of Reading, Earley Gate, P.O. Box 243, Reading, RG6 6BP, United Kingdom.
E-mail: g.zappa@reading.ac.uk

DOI: 10.1175/MWR-D-14-00064.1

von Storch 2008a; Shkolnik and Efimov 2013). However, there is some substantial spread in the number of identified polar lows per year in the different studies. For example, in the Norwegian and Barents Seas, Noer et al. (2011) identify an average number of about 12 polar lows per year in 2000–09 while Blechschmidt (2008) identifies 45 polar lows per year in the same area plus the Labrador Sea in 2004–05. The differences in time period and region do not seem to fully explain the spread in the number of classified polar lows, which can be also affected by the uncertainties in defining what is a polar low (Rasmussen and Turner 2003).

The skill of numerical weather prediction to forecast polar lows improved for model grid spacing of 50 km and finer (Rasmussen and Turner 2003), although the accurate prediction of some events can remain challenging even for model grid spacing finer than 12 km (Aspelien et al. 2011; McInnes et al. 2011). Global atmospheric reanalyses currently have grid spacing comparable or coarser than 50 km and they might therefore not be able to represent polar lows well. Condron et al. (2006) investigated the ability of the 40-yr European Centre for Medium-Range Weather Forecasts (ECMWF) Re-Analysis (ERA-40) to represent a set of satellite-observed polar mesocyclones in the northern North Atlantic region (Harold et al. 1999). They found that ERA-40 shows an associated maximum in surface geostrophic vorticity for 54% of the observed mesocyclones with a higher fraction of missing mesocyclones among those of smaller radius. Therefore, they concluded that ERA-40 highly underestimates the polar mesocyclone activity. Laffineur et al. (2014) found an increased ability of the Interim ECMWF Re-Analysis (ERA-Interim, hereafter ERAI) to represent polar lows compared to ERA-40. However, they suggest ERAI still misses a substantial fraction of polar lows as only 13 of 29 observed polar lows show an associated minimum in mean sea level pressure (MSLP) in ERAI.

This study aims to get further insight into the ability of atmospheric reanalyses to represent polar lows by combining the inspection of observed polar low events (e.g., Laffineur et al. 2014) with the direct identification based on a cyclone-tracking algorithm (e.g., Zahn and von Storch 2008a). Using this joint approach, the ability of the ERAI reanalysis (Dee et al. 2011) and of the ECMWF operational analysis to represent polar lows will be explored and contrasted. The higher horizontal resolution of the operational analysis (~16–25-km grid spacing) compared to the ERAI reanalysis (~80-km grid spacing) will allow the sensitivity of the representation of polar lows to the forecast model resolution to be investigated. In particular, the focus will be on the polar lows of the Norwegian and Barents Seas, where the Sea Surface Temperature and Altimeter Synergy (STARS) dataset of observed polar lows has been recently compiled by the Norwegian Meteorological Services (Noer et al. 2011).

The structure of the paper is as follows. After introducing the data and methods (section 2), the results will be divided into two main parts. In section 3, we compare the representation of the structure and intensity of the observed polar lows listed in STARS between the operational analysis and the ERAI reanalysis. In section 4, we evaluate whether polar lows are sufficiently represented to be directly identified and tracked using a feature-tracking algorithm with objective criteria based on the dynamical intensity of the cyclone and the large-scale environment. The conclusions are presented in section 5.

2. Data and methods

a. ERA-Interim and ECMWF analysis

The ERAI reanalysis (Dee et al. 2011) is a homogeneous atmospheric analysis starting from 1979 and extending up to the present. It is based on the Integrated Forecast System (IFS) cycle 31r2 run with 60 vertical levels and TL255 horizontal spectral resolution. This corresponds to a horizontal grid spacing of about 80 km in the midlatitudes. Observations are assimilated into ERAI using a four-dimensional variational data assimilation scheme with 12-h cycling (Courtier et al. 1994) and output every 6 h.

The representation of polar lows in the ERAI reanalysis will be compared to that in the ECMWF operational analysis system, which was operational from October 2008 to March 2011. Over this period, the operational analysis had several upgrades, namely from IFS cycle 35r1 to 36r4, with improvements in both the forecast model and the data assimilation procedure. Of particular relevance is the horizontal resolution increase from spectral truncation TL799 (~25 km) to TL1279 (~16 km) that became operational on 26 January 2010. Such an increase might have impacts on the representation of polar lows. However, the main conclusions of the paper have been found robust to separately considering the time periods with a constant horizontal resolution. The operational analysis uses 91 vertical levels.

Both the operational analysis and ERAI reanalysis use the Operational Sea Surface Temperature and Sea ice Analysis (OSTIA), apart for the period 1 October 2008–31 January 2009 when ERAI uses the National Centers for Environmental Prediction (NCEP) real-time global sea surface temperature data.

To deal with the short-lived nature of polar lows, data every 3 h is analyzed in this study. As the analyses are only generated every 6 h, the 3-hourly sampling is obtained by combining the analyses with 3- and 9-h ahead forecasts in both ERAI and in the operational analysis.

b. Objective identification and tracking

An objective feature tracking algorithm (Hodges 1995, 1999) is introduced to identify and track polar lows in the reanalysis output. This tracking algorithm has been already applied to the study of tropical cyclones (Bengtsson et al. 2007), synoptic extratropical cyclones (Hoskins and Hodges 2002; Zappa et al. 2013a,b) and, in one previous study, also to polar lows (Xia et al. 2012). However, the specific setup used in this study differs from those discussed in Xia et al. (2012).

Polar lows are identified as relative maxima in the 3-hourly vorticity at 850 hPa with total spectral wavenumbers smaller than 40 and larger than 100 removed. A spectral taper is further applied to reduce the Gibbs oscillations. This T40–T100 filtering focuses on the spatial scales characteristic of mesoscale systems (200–1000 km) while it filters the vorticity associated with synoptic-scale cyclones and small-scale noise. The T40–T100 vorticity maxima above $2 \times 10^{-5}\,s^{-1}$ are then tracked in time by applying constraints on track smoothness and speed. Only tracks with a lifetime of at least 6 h (three time steps) are retained for analysis. The main changes in the tracking algorithm setup relative to the one used for synoptic cyclones are the reduced smoothing of the tracked variable (T40–T100 rather than T5–T42), the increase in the sampling frequency of the data (3-hourly rather than 6-hourly), and adjusted constraints on the smoothness of the tracks to suit with the higher frequency of the data.

A large number of features are identified by the tracking algorithm. For example, about 800 tracks per extended winter (October–March) with maximum T40–T100 vorticity at 850 hPa in the study area (see Fig. 1) are found in the operational analysis. This suggests that besides the polar lows, these tracks may also include other classes of mesocyclones, small-scale synoptic cyclones and frontal features. Therefore, additional criteria need to be applied for extracting the polar lows from the total number of identified tracks (Zahn and von Storch 2008b; Xia et al. 2012). These criteria involve conditions on the static stability of the atmospheric environment, on the size of the cyclones, and on their vorticity and surface wind speed intensities. For clarity, the specific formulation of these criteria is described in section 4.

c. Observed polar lows dataset

The STARS dataset version 2 (Noer et al. 2011) provides a list of hourly tracks of observed polar lows over the Barents and Norwegian Seas from January 2001 to March 2011. The polar lows in the Labrador Sea are also listed from 2006 and the data are available online (http://polarlow.met.no/STARS-DAT/). The STARS polar lows dataset is based on a range of satellite-derived information, including the Advanced Very High Resolution Radiometer (AVHRR) thermal infrared and Quick Scatterometer (QuikSCAT) surface wind speeds, as well as expert judgment from the Norwegian Meteorological Services forecasters. Moreover, a number of additional aspects regarding the large-scale atmospheric environment, such as its static stability and the presence of upper-level advection of potential vorticity and low-level baroclinicity (Noer et al. 2011), are also considered. Only the strongest polar low is reported when a cluster of polar lows forms within the same cold air outbreak (Mallet et al. 2013).

In this study, we will focus on the polar lows of the Barents and Norwegian Seas for three extended winters (October–March) from October 2008 to March 2011, when the operational analysis and ERAI data overlap. In total, 52 polar lows are listed in STARS over this period. The hourly tracks in STARS are subsampled every 3 h at the time steps when reanalysis output data are available. For consistency with the tracking algorithm setup, only the STARS tracks lasting at least three subsampled time steps (a 6-h interval) are retained for analysis. This reduces the number of analyzed STARS polar lows to 34. However, the main conclusions have been found robust to the inclusion of the other short-lived polar lows, and a brief comment on this will be given at the end of section 3.

A spatial map of the genesis and lysis of the analyzed set of STARS polar lows is presented in Fig. 1. As also found in other studies (e.g., Blechschmidt 2008), the majority of polar lows have genesis in the open ocean in the Norwegian and Barents Seas and tend to have lysis on the Scandinavian coast.

3. Direct identification of observed polar lows

In this section, the representation of the STARS polar lows in the operational analysis and in the ERAI reanalysis is examined. This will allow us to evaluate the extent that ERAI represents polar lows, and how sensitive their representation might be to an increase in the forecast model resolution. Initially, a case study will be analyzed in detail. Afterward, some key polar low characteristics will be compared between the operational analysis and ERAI across the whole STARS dataset.

a. Case study

A polar low formed north of Iceland, in the Denmark Strait, on the night between 21 and 22 March 2011. A near infrared (841–867 nm) satellite image of the polar low at 1157 UTC on 22 March is presented in Fig. 2a. In the satellite image, the polar low features high spiraling clouds, particularly on the northern and eastern sides, and a relatively well-defined center. The polar low formed

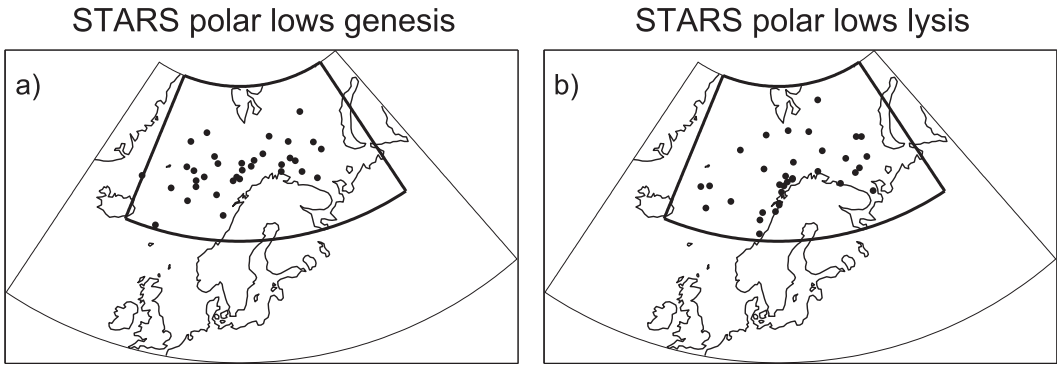

FIG. 1. (a) Genesis and (b) lysis locations of the subset of polar lows listed in STARS between October 2008 and March 2011, which are considered in this study. The genesis and lysis are evaluated at the time steps available in the 3-hourly ERAI output. The black box (latitude 64°–80°N and longitude 15°W–60°E) defines the study area. Only the tracked and STARS polar lows reaching maximum vorticity intensity within the box are considered in this study.

under the influence of a north westerly cold air advection whose influence can be still seen in the cloud streets of oceanic cellular convection located northeast of the polar low in Fig. 2a.

At the closest time relative to the satellite image (1200 UTC), the ERAI MSLP shows high pressure over the United Kingdom and Greenland, and low pressure in the Barents and Arctic Seas (see Fig. 2b). This quadrupole pattern is responsible for the northerly cold air advection mentioned above. Moreover, closed isobars and a localized minimum in MSLP can be found at the polar low location, which suggests ERAI is able to represent the surface cyclonic circulation associated with the polar low. After its genesis, as reported in STARS, the polar low propagated eastward and it reached the northern coast of Norway in about 33 h, where it dissipated (see Fig. 2b).

To evaluate the extent that ERAI captures the structure of the polar low, the represented vorticity, wind speed, and thermal structure will be analyzed and compared to that found in the operational analysis. These fields are presented in Figs. 3a–h for spherical caps of 5° of radius (~500 km) centered on the polar low position given in STARS at 1200 UTC 22 March.

In the operational analysis a region of positive vorticity is found at the STARS polar low location (Fig. 3a). Moreover, positive vorticity is also organized in a narrow spiraling filament extending from the polar low center toward the southeast. This feature corresponds to a surface occluded front and it is consistently similar to the shape of the cloud band of the polar low seen in the satellite image (cf. Fig. 2a). Therefore, the operational analysis appears to represent the polar low well, in terms of its associated low-level cyclonic circulation and its mesoscale structure.

ERAI also shows a region of positive 850-hPa vorticity at the location of the observed polar low and a spiraling filament of positive vorticity associated with the surface front (Fig. 3b). However, the vorticity field is much smoother and it is less similar to the polar low cloud structure. This suggests that although ERAI represents the observed polar low, it has only limited ability to resolve the polar low structure.

In section 4, polar lows will be directly tracked as maxima in the T40–T100 filtered vorticity at 850 hPa. It is, therefore, of interest to validate whether the tracked variable is appropriate for this purpose. For the case study, we find a maximum in the T40–T100 vorticity at the polar low location in both the operational analysis and ERAI (Figs. 3c,d). Moreover, the T40–T100 filter smooths the vorticity associated with the surface front, while retaining a clear signal associated with the polar low center. On the basis of this test case, the T40–T100 smoothed vorticity is fit for the purpose of tracking polar lows. It is also of interest to note that the T40–T100 vorticity is very similar between the operational analysis and ERAI. Therefore, despite the differences found in the full resolution vorticity, the operational analysis and ERAI have similar vorticity structures at these spatial scales.

The 925-hPa wind speed is shown in Figs. 3e,f. Wind speeds stronger than $30\,m\,s^{-1}$ are found in the operational analysis approximately 100 km southwest of the polar low center. ERAI does not capture the wind speed location and intensity found in the operational analysis, the wind speed peak being about $2\,m\,s^{-1}$ weaker and located 100 km farther from the polar low center compared to the operational analysis. This confirms the limits of ERAI in representing the structure of this polar low.

The difference between the temperature at 500 hPa and the sea surface temperature (T500 − SST) is presented in Figs. 3g,h. Values in T500 − SST smaller

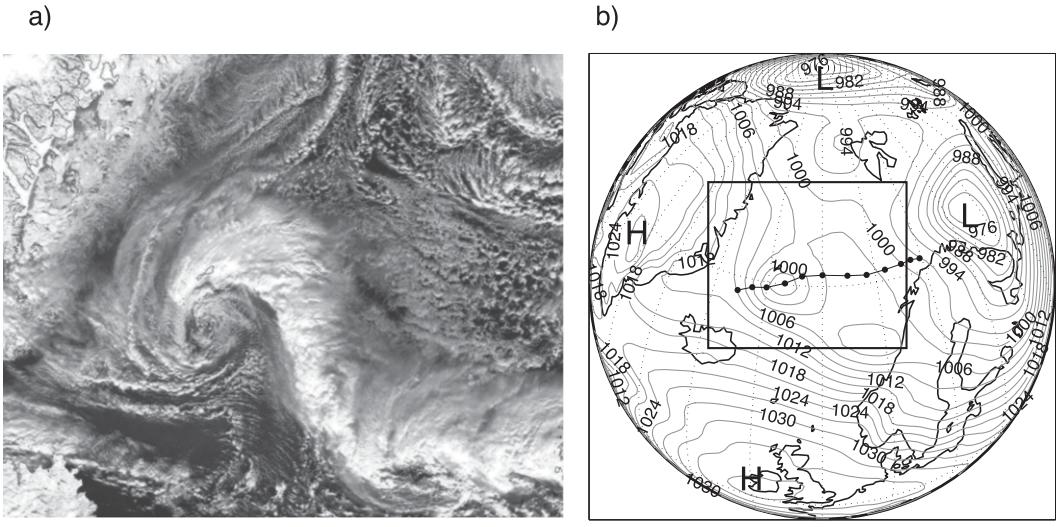

FIG. 2. (a) Near-infrared (841–867 nm) image taken at 1157 UTC 22 Mar 2011 from the Moderate Resolution Imaging Spectroradiometer (MODIS). The image has been obtained from the Dundee satellite receiving station. (b) MSLP in ERAI at 1200 UTC on the same day. Units are in hPa and the contour interval is 3 hPa. The black dots indicate the polar low position every 3 h and the black line indicates its track. The rectangular box delimits the area captured by the satellite image in Fig. 2a. The high (H) and low (L) MSLP regions are indicated.

than −43° have been found to typically characterize the cold air outbreak environments that are most favorable to polar low development (Zahn and von Storch 2008b; Bracegirdle and Gray 2008; Noer et al. 2011). The operational analysis and ERAI have a similar representation of T500 − SST and values below −43° are found close to and northeast of the polar low center. This spatial structure results from the superposition of colder midtropospheric air to the north of the polar low, associated with the cold air advection, and warmer SST to the east, associated with the warm influence of the Norwegian coastal current.

b. *STARS dataset*

The previous analysis examined the case of a polar low represented in both the operational analysis and ERAI reanalysis and it showed there are differences in the associated vorticity and wind speed fields. In this section we further explore to what extent these findings apply to the other observed polar lows listed in STARS.

The representation of the STARS polar lows in the operational analysis and ERAI is first investigated by looking for local maxima in the T40–T100 vorticity at 850 hPa collocated with the polar lows in STARS. The local maxima are searched by steepest ascent starting from the polar low position given in STARS up to a maximum distance of 2.5°. In both the operational analysis and ERAI, a well-defined collocated maximum in the T40–T100 vorticity is found for 33 of the 34 polar lows in STARS, while the remaining polar low (number 139 in STARS-v2 dataset) does not show a clear collocated signal in the T40–T100 vorticity. Moreover, there are three polar lows in ERAI and two polar lows in the operational analysis that miss a collocated maximum in the T40–T100 vorticity at one or two time steps, suggesting that the life cycles might not be always well represented.

A scatterplot of the alongtrack maximum T40–T100 vorticity at 850 hPa in the ERAI reanalysis against the operational analysis is presented in Fig. 4a for the 33 polar lows with a well-defined collocated surface maximum in T40–T100 vorticity. According to this metric, ERAI generally underestimates the intensity of polar lows compared to the operational analysis, with differences that are of the order of $10^{-5}\,s^{-1}$. In both the datasets, the frequency distribution of the vorticity intensity peaks at about $9 \times 10^{-5}\,s^{-1}$ (see Fig. 4b).

The analysis presented for the T40–T100 vorticity intensity is now extended to the alongtrack maximum of the surface wind speed maximum associated with the polar lows (see Fig. 5). The surface wind speed maximum is searched within 2.5° relative to the T40–T100 vorticity maximum. In the operational analysis, the surface wind speeds are typically in the range of 15–25 $m\,s^{-1}$. Consistent with the vorticity intensity results, the surface wind speeds in ERAI are weaker than in the operational analysis (see Fig. 5a), with a typical underestimation of about 2 $m\,s^{-1}$. The number of polar lows associated with the most extreme wind speeds (~25 $m\,s^{-1}$) is more than 50% less in ERAI compared to the operational analysis.

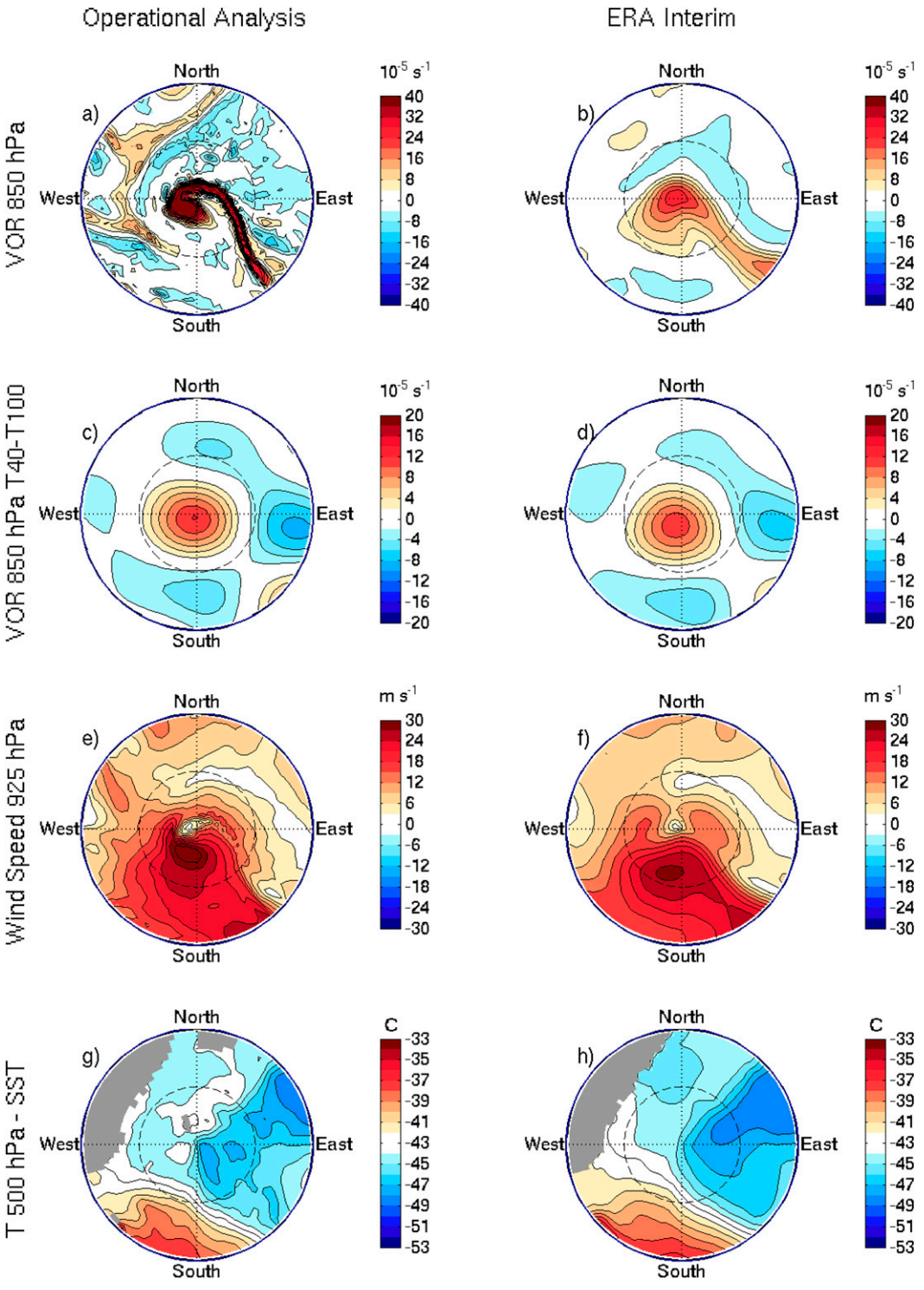

FIG. 3. Maps of (a),(b) 850-hPa vorticity; (c),(d) 850-hPa vorticity smoothed to T40–T100 resolution; (e),(f) wind speed at 925 hPa; and (g),(h) of the difference between the temperature at 500 hPa and the SST presented for 5° radial caps centered on the polar low case study position at 1200 UTC 22 Mar 2011. The maps are presented for both the (a),(c),(e),(g) ECMWF operational analysis and for (b),(d),(f),(h) ERAI. In (g) and (h) land and sea ice regions are masked gray. Units are (a)–(d) $10^{-5}\,s^{-1}$; (e),(f) $m\,s^{-1}$; and (g),(h) °C.

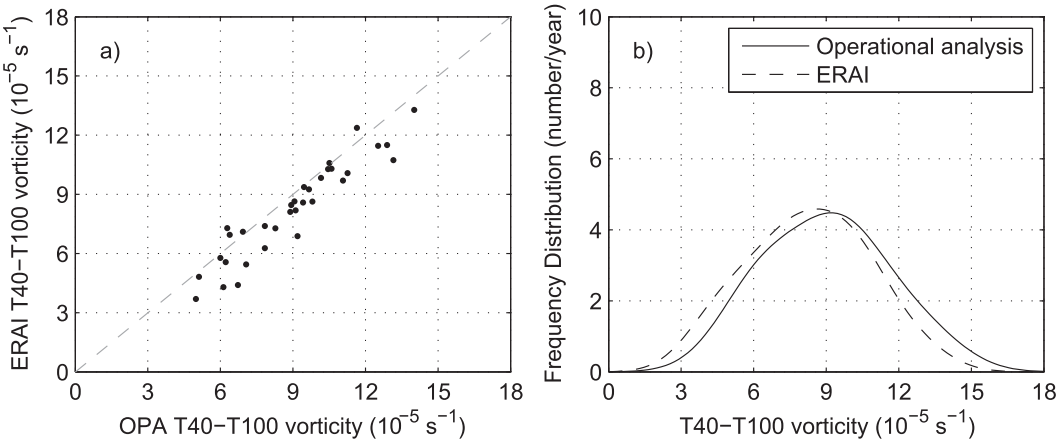

FIG. 4. (a) Scatterplot of the peak T40–T100 vorticity at 850 hPa associated with the STARS polar lows as represented in ERAI (ERAI) against the ECMWF operational analysis (OPA). (b) Kernel smoothed frequency distribution of the peak T40–T100 vorticity at 850 hPa of the STARS polar lows as represented in ERAI (full line) and in the operational analysis (dashed line). The STARS polar low missing a well-defined T40–T100 vorticity maximum in both ERAI and the operational analysis (see the text) is not included in the figure.

Moreover, nine polar lows in ERAI do not reach the 15 m s^{-1} threshold that is commonly required to classify an observed polar mesocyclone as a polar low (Rasmussen and Turner 2003). This provides further evidence for the underestimation of wind speeds in ERAI. We also find that four polar lows have surface wind speeds slightly below the 15 m s^{-1} threshold in the operational analysis as well.

In summary, both the operational analysis and the ERAI show the 850-hPa vorticity signature of a collocated mesocyclone associated with all but one the STARS polar lows of lifetime of at least 6 h. This result does not seem to be highly sensitive to the lifetime of the polar lows, and a collocated maximum in the T40–T100 vorticity is also found for seven of the eight STARS polar lows with lifetime below 6 h and that include one ERAI time step. The ability of the operational analysis and ERAI to represent polar lows suggests that it might be possible to directly identify and track them as maxima in the filtered 850-hPa vorticity field. However, some limitations may arise, particularly in ERAI, from the underestimation of the polar low wind speed and vorticity intensities, which may make it difficult to separate them from other mesocyclones. This will be addressed in the next section.

4. Tracking of polar lows

a. *Identification criteria*

In the operational analysis, about 800 tracks per extended winter season are found by the tracking algorithm in the Norwegian and Barents Seas as maxima in the T40–T100 vorticity at 850 hPa. This large number implies that additional criteria are needed to identify the subset of polar lows. Most of the criteria employed here are related to those applied in previous studies (Zahn and von Storch 2008b; Bracegirdle and Gray 2008).

A commonly required criterion is that T500 − SST is lower than −43° in the vicinity of the polar low (Zahn and von Storch 2008b). T500 − SST is here evaluated as the difference between the 1° radius area average of T500 and SST centered at the location of the T40–T100 850-hPa vorticity maximum. Furthermore, to comply with the condition that polar lows are intense mesocyclones, we verify that the surface absolute wind speed maximum within 2.5° radius exceeds 15 m s^{-1} (Rasmussen and Turner 2003). The wind speed maximum is required to be found in the interior of the 2.5° search area rather than on the border. Therefore, this also provides a constraint on the size of the tracked cyclone. To do this more accurately, the wind speed field is first spline interpolated to a grid in polar coordinates with the pole centered on the T40–T100 vorticity maximum and resolution of 3° in the angular coordinate and 0.25° (~25 km) in the radial coordinate.

The wind speed condition alone does not guarantee that the feature is a polar low, as cold air outbreaks can have background flows of 15 m s^{-1} or more even in the absence of any polar low (Noer et al. 2011). We, therefore, further require that the T40–T100 vorticity at 850 hPa is higher than 6×10^{-5} s^{-1}. The chosen, arbitrary, threshold is motivated by the fact that most of the STARS polar lows reach this vorticity intensity in the operational analysis

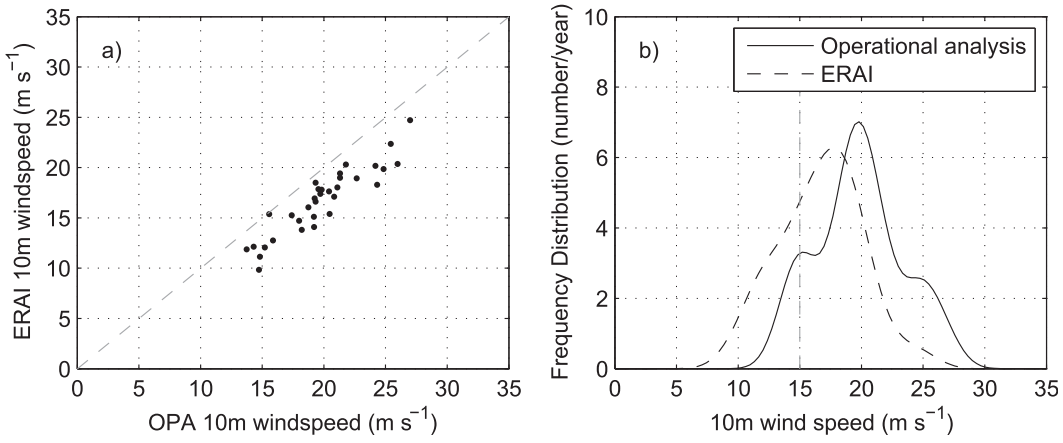

FIG. 5. As in Figs. 4a,b but for the maximum along–track peak wind speed at 10 m associated with the STARS polar lows.

(see Fig. 4). The sensitivity to this threshold will be discussed in section 4d. Finally, the track is required to predominantly occur over the ocean.

In summary, the following identification criteria need to be verified for classifying a track as a polar low:

- T500 − SST $< -43°$, averaged over a 1° radius.
- Surface wind speed max $>15\,\mathrm{m\,s^{-1}}$ within a 2.5° radius.
- T40–T100 vorticity at 850 hPa $>6 \times 10^{-5}\,\mathrm{s^{-1}}$.
- Ocean fraction greater than 75%, averaged over a 1° radius.

For each track, the above identification criteria are requred to be satisfied at a common time step when the along track T40–100 vorticity reaches a relative maximum.

Laffineur et al. (2014) suggest caution in tracking polar lows using vorticity, as vorticity maxima can be also associated with troughs but not necessarily closed mesocyclonic circulation. However, our results (sections 4b–4d) suggest that the spatial filtering and the set of identification criteria are effective at rejecting the identification of troughs. On the other hand, we choose to not require the presence of an associated closed minimum in MSLP as its emergence can be influenced by the specific synoptic conditions in which the polar low forms and in particular by the strength of the background pressure gradient.

For clarity, the tracking and identification results are first presented for the operational analysis (sections 4b–4d). The identification of polar low tracks in ERAI, and a comparison to the operational analysis, will be then discussed in section 4e.

b. *Tracking results: Operational analysis*

Of the tracks found in the operational analysis, we identify 72 tracks that meet the polar low identification criteria in the three extended winters from October 2008 to March 2011. This is roughly twice the number of polar lows of at least 6-h lifetime listed in STARS over the same period.

Track to track matching is applied to identify the tracked polar lows in the operational analysis that are also listed in STARS, those that are not listed in STARS and the STARS polar lows that are not identified by the tracking (misses). The matching condition requires a time overlap of at least 50% of the STARS track lifetime and a time average distance smaller than 2.5° (~250 km) in the overlapping period. This threshold is motivated by the typical radius of polar lows.

We find that of the 72 identified polar low tracks in the operational analysis 23 are also listed in STARS while 49 are not listed in STARS (see Table 1). The nature of the identified tracks not listed in STARS will be discussed in section 4c. Moreover, there are 11 STARS polar lows (i.e., ~32% of STARS), which are not found among the identified polar low tracks in the operational analysis. However, the number of missed STARS polar lows decreases to 6 if the initial set of tracks, before the identification criteria are applied, is considered. Therefore, 5 of the 11 missed STARS polar lows show an 850-hPa vorticity track in the operational analysis, but they are not identified because their representation does not satisfy the objective identification criteria.

In general, we find that 10 of the 34 STARS polar lows have a representation in the operational analysis that does not satisfy the objective criteria (see Table 2). In particular, there are three polar lows that do not satisfy the vorticity intensity condition and five that do not satisfy the wind speed intensity condition. This implies that some polar lows in STARS can be missed by the identification algorithm because they are too weak in the operational analysis relative to our identification criteria.

TABLE 1. Number of identified polar low tracks in the operational analysis (OPA) and in ERA-Interim (ERAI) by applying the objective criteria and results from the track-to-track matching against the polar lows listed in STARS. Column 1 gives the dataset. Column 2 gives the total number of identified polar lows. Column 3 gives the number of identified polar lows that are listed in STARS, and column 4 gives the number of those that are not listed in STARS. Column 5 gives the total number (and fraction) of STARS polar lows that are not included among the identified polar lows (misses).

Dataset	Identified	Listed in STARS	Not listed in STARS	Missed STARS
OPA	72	23	49	11 out of 34 (~30%)
ERAI	51	19	32	15 out of 34 (~45%)

There are also four polar lows with T500 − SST values between −40° and −43°C so that they fail to pass the static stability criterion. Finally, there is also one polar low that satisfies all the different criteria, but on different time steps.

These results show that a polar low dataset from the operational analysis based on this setup of the identification and tracking algorithm would miss a considerable fraction (~30%) of observed polar lows. Some of these misses might be due to the operational analysis not being good enough (e.g., those due to too weak wind speeds). Others might be due to the tested criteria being critical, but not universal, properties of polar lows (e.g., the condition on T500 − SST). Relaxing the thresholds of the criteria would lead the number of misses to decrease, but it would also lead to the identification of additional features which would unlikely be polar lows.

c. *What are the "not listed in STARS" tracks?*

Of the 72 identified polar low tracks in the operational analysis, we find that 49 are not listed in STARS (see Table 1). Understanding the nature of these features is important for having a reliable identification of polar lows.

Thermal infrared satellite images of two identified polar lows in the operational analysis not listed in STARS are presented in Fig. 6. In both cases, the cloud vortexes characteristic of polar lows can be identified in the satellite images. Comma-shape or spiraliform cloud patterns have also been typically identified in other inspected tracks not listed in STARS (not shown) and particularly for those of higher T40–T100 vorticity intensity. This would suggest that these additional identified tracks not listed in STARS may also be interpreted as polar lows.

This interpretation is consistent with the finding that the 72 (~24 per extended winter) Norwegian and Barents Seas polar lows identified in the operational analysis is within the range of observational uncertainty from previous studies. For example, Blechschmidt (2008), using a satellite-based approach, identifies about 30 polar lows per extended winter in a 2-yr period (2004–05) in the area analyzed in this study. In a similar area, Zahn and von Storch (2008a), using an identification and tracking algorithm applied to downscaled NCEP–National Center for Atmospheric Research (NCAR) reanalysis data, estimate an average of about 25 polar lows per year over the 1960–2000 period.

A possible reason why the STARS climatology shows lower polar low numbers than other studies might be related to the choice of reporting only the most intense polar lows for each cluster of polar lows that are part of the same cold air outbreak event (Mallet et al. 2013). Consistently, about 55% of the identified polar low tracks not listed in STARS have a maximum intensity that occurs within 2 days and less than 1000 km relative to the genesis of a STARS polar low.[1]

d. *Sensitivity to the vorticity intensity threshold*

To explore the sensitivity of the $6 \times 10^{-5}\,s^{-1}$ threshold on T40–T100 vorticity intensity at 850 hPa, the objective identification and the track-to-track matching statistics presented in Table 1 have been recomputed for different vorticity intensity thresholds. For the operational analysis, the results are shown in Fig. 7a, where the number of identified polar lows (gray line) is presented for a range of T40–T100 vorticity intensity thresholds between 3×10^{-5} and $13 \times 10^{-5}\,s^{-1}$. As in Table 1, the number of identified polar lows is further decomposed between the fraction that is also listed in STARS (dark shading) and the fraction that is not (light shading). The black line gives the number of STARS polar lows reaching that vorticity intensity in the operational analysis.

As expected, increasing the vorticity intensity threshold leads to a reduction in both the number of polar lows identified in the operational analysis (gray line) and in the number of STARS polar lows reaching that intensity (black line). However, in the intensity range between 3×10^{-5} and $6 \times 10^{-5}\,s^{-1}$ there is a 30% reduction in the number of identified polar lows in the operational analysis but a very small change in the number of STARS polar lows reaching that vorticity intensity. This highlights how introducing a threshold on vorticity intensity of $6 \times 10^{-5}\,s^{-1}$ is likely to filter out a number of vorticity features associated with weak cyclonic disturbances along intense cold air outbreaks.

By increasing the vorticity threshold from 6×10^{-5} to $13 \times 10^{-5}\,s^{-1}$, the number of identified polar lows

[1] STARS polar lows of any lifetime are considered in this estimate.

TABLE 2. Number of STARS polar lows whose representation in the ECMWF operational analysis (OPA) and in ERA-Interim (ERAI) does not satisfy the identification criteria for polar lows tested by the tracking algorithm. Column 1 gives the dataset. Column 2 gives the number of STARS polar lows that do not satisfy at least one criterion. Columns 3–5 separately quantify the number of polar lows not fulfilling the criteria on vorticity intensity, wind speed intensity, and atmospheric static stability, respectively. Column 6 shows the number of polar lows that satisfy the different criteria at different time steps but not at the same one.

		Individual criteria			
Dataset	Any criteria	Vorticity $< 6 \times 10^{-5}\,s^{-1}$	Wind $< 15\,m\,s^{-1}$	T500 − SST $> -43°$	Time step
OPA	10 out of 34	3	5	4	1
ERAI	14 out of 34	8	9	3	1

(gray line) and of STARS polar lows (black line) tend to become similar and they show very similar numbers for vorticity thresholds greater or equal than $10 \times 10^{-5}\,s^{-1}$. Consistently, both the fraction of identified polar lows not listed in STARS and the fraction of missed STARS polar lows (i.e., the gap between the black line and the dark shading) tend to decrease. These results suggest that good agreement can be obtained between a vorticity-tracking-based and a satellite-based polar low dataset for the top 30% most intense events as measured by vorticity. It is possible that this behavior is related to the definition itself of polar lows as intense polar mesocyclones, as this implies that polar lows are better defined at higher dynamical intensity.

e. *Tracking results: ERA-Interim*

In general, the identification and tracking of polar lows in ERAI shows qualitatively similar results to those already presented for the operational analysis. Table 1 shows that both the tracking of polar lows in ERAI and in the operational analysis is characterized by a substantial number of identified polar lows not listed in STARS and of missed STARS polar lows. Moreover, there is a convergence between the set of identified polar lows in ERAI and the STARS polar lows for increasing thresholds on vorticity intensity, which is similar, although even stronger, to that already discussed for the operational analysis (cf. Figs. 7a and 7b). However, some important quantitative differences between ERAI and the operational analysis are found.

Using the $6 \times 10^{-5}\,s^{-1}$ threshold on vorticity, 51 polar low are identified in ERAI over the three extended winter periods (2008–11). This is about 20% less than the number of polar lows identified in the operational analysis (see Table 1). Moreover, the set of identified polar lows in ERAI includes about 55% of the STARS polar lows, which is again less than the ~70% of STARS polar lows found by the identification and tracking algorithm in the operational analysis (see Table 1).

This reduction in the number of identified polar lows in ERAI is largely due to the weaker representation of 850-hPa vorticity and surface wind speed intensities compared to the operational analysis. This implies that the criteria for polar low identification are less frequently satisfied in ERAI. For example, we find that eight STARS polar lows have a representation in ERAI that does not satisfy the $6 \times 10^{-5}\,s^{-1}$ vorticity intensity condition and nine STARS polar lows have a representation that does not satisfy the $15\,m\,s^{-1}$ condition on surface wind speed (see Table 2). This is about the double of the number of STARS polar lows not satisfying the same criteria in the operational analysis.

The tracking of polar lows in ERAI has also been extended to the whole STARS period (i.e., the nine extended winters from October 2002 to March 2011). All the discussed results are confirmed when inspecting this longer time period, which is characterized by a smaller average number of polar lows per year in both ERAI (−20%) and listed in STARS (−26%) compared with 2008–11.

5. Conclusions

In this work we have explored how the polar lows of the Norwegian and Barents Seas listed in STARS are represented in the ECMWF operational analysis and in ERAI. Moreover, the possibility of directly identifying and tracking polar lows in the ERAI and operational analysis has been investigated by applying an objective identification and tracking algorithm which has been validated against STARS.

The main findings of the paper are the following:

1) Both the operational analysis and ERAI show the vorticity signature of a surface mesocyclone collocated with 33 of the 34 observed STARS polar lows with a lifetime of at least 6 h, although the life cycles are in few cases not fully captured.
2) The operational analysis is better able to resolve the mesoscale structure of polar lows and has stronger wind speeds compared to ERAI. This is consistent with the three times higher horizontal resolution of the operational analysis compared to ERAI.

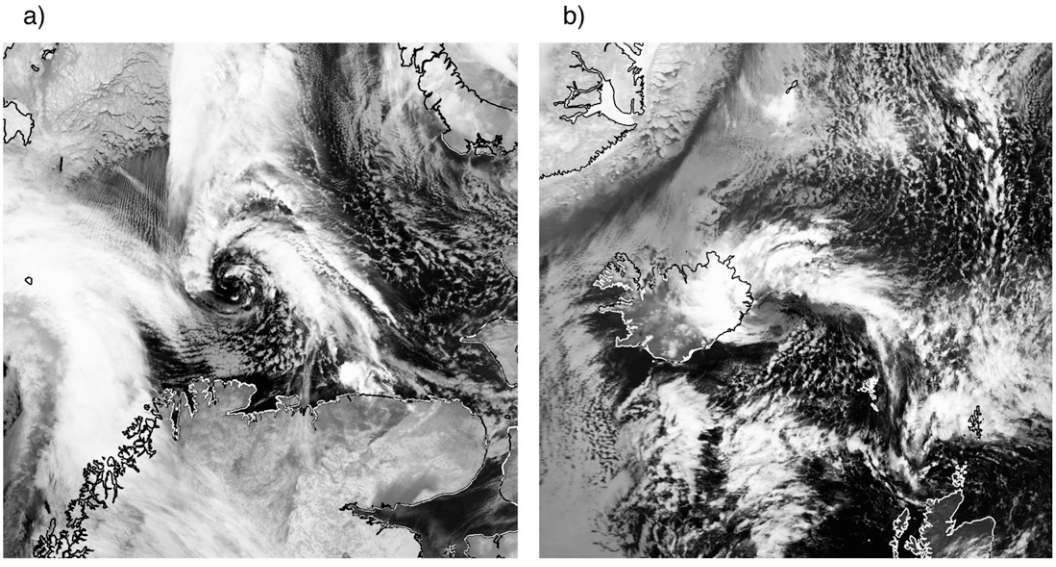

FIG. 6. Thermal infrared (10.3–11.3 μm) satellite images taken from the AVHRR instrument and obtained from the Dundee satellite receiving station of two polar lows identified in the operational analysis but not listed in STARS. (a) 0920 UTC 8 Jan 2009, a polar low is located northeast of North Cap, and (b) 0245 UTC 29 Mar 2010 a polar low is located just east of Iceland.

3) For about 30% (9 of 34) of the STARS polar lows, the represented surface wind speeds in ERAI is below the 15 m s^{-1} threshold, which is characteristic of polar lows. Four STARS polar lows have wind speeds just below 15 m s^{-1} also in the operational analysis. Furthermore, the number of polar lows associated with intense surface wind speeds (~25 m s^{-1}) is more than 50% smaller in ERAI compared to the operational analysis. These results suggest that ERAI is likely to underestimate the surface wind speeds associated with polar lows.
4) A tracking algorithm with objective identification criteria identifies 23 of the 34 polar lows listed in STARS in the operational analysis, and 19 of 34 in ERAI. The remaining polar lows, particularly in ERAI, are largely missed because they do not satisfy the identification criteria on wind speed, vorticity, and static stability tested by the algorithm, although tracks are found for many of them. In particular, the weaker wind speed and vorticity intensities in ERAI compared to the operational analysis explain the different fraction of identified STARS polar lows between the two datasets. Overall, about 20% less polar low tracks are identified in ERAI in comparison to the operational analysis according to the identification criteria.

The tracking and identification algorithm identifies more polar lows than there are listed in STARS. This is particularly true for polar lows of lower intensity in vorticity. However, excellent agreement between the objectively identified polar lows and STARS is found for the strongest 30% polar lows in vorticity in both ERAI and the operational analysis. This suggests that part of the difference in number of the identified polar low tracks and STARS is related to drawing the boundary between polar mesocyclones and polar lows. This uncertainty in evaluating what mesocyclones should be classified as polar lows can affect any polar low climatology and it may explain some of the spread in the number of polar lows listed in different observational datasets.

Our findings on ERAI are broadly consistent with the recent analyses of Laffineur et al. (2014), although two different time periods have been analyzed. Laffineur et al. (2014) find that ERAI captures 13 out of 29 (~40%) observed polar lows, as revealed by the presence of an associated close minimum in MSLP. The fraction identified in ERAI using our identification criteria is ~55%. When interpreting these numbers it is important to consider that ERAI shows the vorticity signature of a mesocyclone for the majority of observed polar lows. Therefore, the number of "captured" polar lows depends on how accurately they are expected to be represented in the reanalysis or, in other terms, on what morphological features are required to be found. Examples of these morphological features are a closed minimum in MSLP, as required by Laffineur et al. (2014), or intense surface wind speeds and vorticity, as required in this study.

The ability of ERAI to represent polar lows is encouraging given its relatively coarse resolution. However, the underestimation of the dynamical intensities of polar lows, and the consequent underestimation in the number

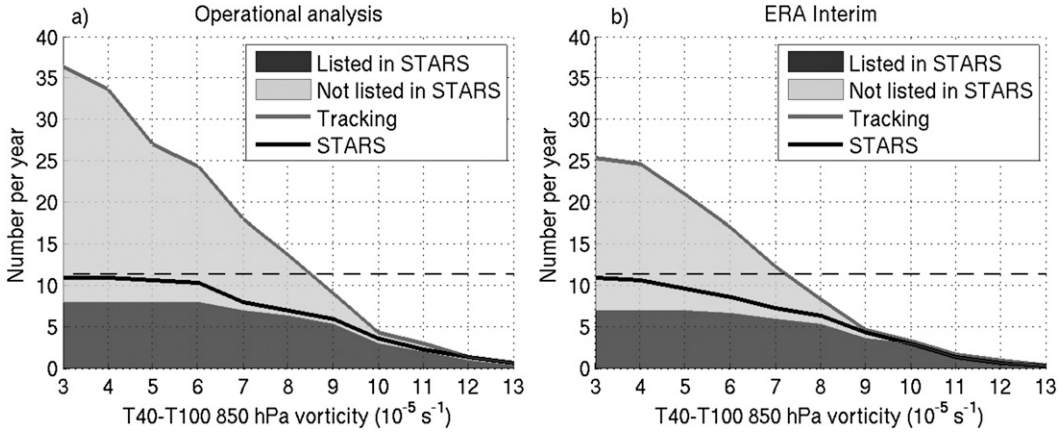

FIG. 7. Number of tracked (gray line) and STARS (black line) polar lows having T40–T100 vorticity intensity above the threshold given in the *x* axis in the (a) operational analysis and in (b) ERAI. The number of identified polar lows is further decomposed in the fraction that is also listed in STARS (dark shading) and those that are not (light shading). The black dashed line marks the level of the total number of polar lows in STARS independently from the intensity threshold.

of identified polar lows relative to the operational analysis, suggests that ERAI may still not be good enough for many polar low related studies and applications. For example, the represented surface heat fluxes over high-latitude oceans might still be too weak compared to observations, which would have implications for using ERAI to drive ocean models (Condron and Renfrew 2013). Furthermore, the difference in the number of identified polar lows between the operational analysis and ERAI suggests that a climatology of polar lows derived from ERAI using the tracking algorithm would be affected by these deficiencies. This can be a main issue, for example, for the use of the ERAI climatology to validate the representation of polar lows in high-resolution climate models (e.g., Kinter et al. 2013). On the other hand, preliminary analyses (not shown) suggest that the relationship between the development of polar lows in ERAI and the large-scale atmospheric circulation is very similar to that found by Mallet et al. (2013) using shorter observational datasets of polar lows. Therefore, ERAI could have some value to better understand the role of precursors in polar lows formation (Blechschmidt et al. 2009; Kolstad 2011).

Future work will have to extend these analyses to other polar low active basins, such as the Labrador Sea and the Sea of Japan (Yanase et al. 2002). Furthermore, it would be of interest to compare the representation of polar lows in ERAI to that in the NCEP Climate Forecast System (CFS) reanalysis (~40-km resolution coupled reanalysis), which shows very few Norwegian Sea polar lows according to Shkolnik and Efimov (2013). Finally, the tracking algorithm could be used to analyze the 3D composite structure and life cycle of polar lows in the operational analysis and validate the structure and number of polar lows in high-resolution climate models.

Acknowledgments. We are very grateful to the Norwegian Meteorological Services for producing and making available the STARS polar lows dataset, to the ECMWF for the ERA-Interim and operational analysis data and to the "NEODAAS/University of Dundee" for providing the satellite images. We would also like to acknowledge Sue Gray for the insightful discussions. This work is part of the Testing and Evaluating Model Prediction of European Storms (TEMPEST) project that is funded by NERC. We finally acknowledge NCAS for the financial support.

REFERENCES

Aspelien, T., T. Iversen, J. B. Bremnes, and I.-L. Frogner, 2011: Short-range probabilistic forecasts from the Norwegian limited-area EPS: Long-term validation and a polar low study. *Tellus,* **63A,** 564–584, doi:10.1111/j.1600-0870.2010.00502.x.

Bengtsson, L., K. I. Hodges, and M. Esch, 2007: Tropical cyclones in a T159 resolution global climate model: Comparison with observations and re-analyses. *Tellus,* **59A,** 396–416, doi:10.1111/j.1600-0870.2007.00236.x.

Blechschmidt, A.-M., 2008: A 2-year climatology of polar low events over the Nordic Seas from satellite remote sensing. *Geophys. Res. Lett.,* **35,** L09815, doi:10.1029/2008GL033706.

——, S. Bakan, and H. Graßl, 2009: Large-scale atmospheric circulation patterns during polar low events over the Nordic seas. *J. Geophys. Res.,* **114,** D06115, doi:10.1029/2008JD010865.

Bourassa, M. A., and Coauthors, 2013: High-latitude ocean and sea ice surface fluxes: Challenges for climate research. *Bull. Amer. Meteor. Soc.,* **94,** 403–423, doi:10.1175/BAMS-D-11-00244.1.

Bracegirdle, T. J., and S. L. Gray, 2008: An objective climatology of the dynamical forcing of polar lows in the Nordic seas. *Int. J. Climatol.,* **28,** 1903–1919, doi:10.1002/joc.1686.

Businger, S., 1985: The synoptic climatology of polar low outbreaks. *Tellus,* **37A,** 419–432, doi:10.1111/j.1600-0870.1985.tb00441.x.

Condron, A., and I. A. Renfrew, 2013: The impact of polar mesoscale storms on northeast Atlantic Ocean circulation. *Nat. Geosci.,* **6,** 34–37, doi:10.1038/ngeo1661.

——, G. R. Bigg, and I. A. Renfrew, 2006: Polar mesoscale cyclones in the Northeast Atlantic: Comparing climatologies from ERA-40 and satellite imagery. *Mon. Wea. Rev.,* **134,** 1518–1533, doi:10.1175/MWR3136.1.

——, ——, and ——, 2008: Modeling the impact of polar mesocyclones on ocean circulation. *J. Geophys. Res.,* **113,** C10005, doi:10.1029/2007JC004599.

Courtier, P., J. N. Thépaut, and A. Hollingsworth, 1994: A strategy for operational implementation of 4D-Var, using an incremental approach. *Quart. J. Roy. Meteor. Soc.,* **120,** 1367–1387, doi:10.1002/qj.49712051912.

Dee, D. P., and Coauthors, 2011: The ERA-Interim reanalysis: Configuration and performance of the data assimilation system. *Quart. J. Roy. Meteor. Soc.,* **137,** 553–597, doi:10.1002/qj.828.

Harold, J. M., G. R. Bigg, and J. Turner, 1999: Mesocyclone activity over the Northeast Atlantic. Part 1: Vortex distribution and variability. *Int. J. Climatol.,* **19,** 1187–1204, doi:10.1002/(SICI)1097-0088(199909)19:11<1187::AID-JOC419>3.0.CO;2-Q.

Hodges, K. I., 1995: Feature tracking on the unit sphere. *Mon. Wea. Rev.,* **123,** 3458–3465, doi:10.1175/1520-0493(1995)123<3458:FTOTUS>2.0.CO;2.

——, 1999: Adaptive constraints for feature tracking. *Mon. Wea. Rev.,* **127,** 1362–1373, doi:10.1175/1520-0493(1999)127<1362:ACFFT>2.0.CO;2.

Hoskins, B., and K. Hodges, 2002: New perspectives on the Northern Hemisphere winter storm tracks. *J. Atmos. Sci.,* **59,** 1041–1061, doi:10.1175/1520-0469(2002)059<1041:NPOTNH>2.0.CO;2.

Kinter, J. L., III, and Coauthors, 2013: Revolutionizing climate modeling with Project Athena: A multi-institutional, international collaboration. *Bull. Amer. Meteor. Soc.,* **94,** 231–245, doi:10.1175/BAMS-D-11-00043.1.

Kolstad, E. W., 2011: A global climatology of favourable conditions for polar lows. *Quart. J. Roy. Meteor. Soc.,* **137,** 1749–1761, doi:10.1002/qj.888.

——, and T. J. Bracegirdle, 2008: Marine cold-air outbreaks in the future: An assessment of IPCC AR4 model results for the Northern Hemisphere. *Climate Dyn.,* **30,** 871–885, doi:10.1007/s00382-007-0331-0.

Laffineur, T., C. Claud, J.-P. Chaboureau, and G. Noer, 2014: Polar lows over the Nordic Seas: Improved representation in ERA-Interim compared to ERA-40 and the impact on downscaled simulations. *Mon. Wea. Rev.,* **142,** 2271–2289, doi:10.1175/MWR-D-13-00171.1.

Mallet, P. E., C. Claud, C. Cassou, G. Noer, and K. Kodera, 2013: Polar lows over the Nordic and Labrador Seas: Synoptic circulation patterns and associations with North Atlantic–Europe wintertime weather regimes. *J. Geophys. Res. Atmos.,* **118,** 2455–2472, doi:10.1002/jgrd.50246.

McInnes, H., J. Kristiansen, J. E. Kristjánsson, and H. Schyberg, 2011: The role of horizontal resolution for polar low simulations. *Quart. J. Roy. Meteor. Soc.,* **137,** 1674–1687, doi:10.1002/qj.849.

Noer, G., Ø. Saetra, T. Lien, and Y. Gusdal, 2011: A climatological study of polar lows in the Nordic Seas. *Quart. J. Roy. Meteor. Soc.,* **137,** 1762–1772, doi:10.1002/qj.846.

Rasmussen, E. A., and J. Turner, 2003: *Polar Lows: Mesoscale Weather Systems in the Polar Regions*. Cambridge University Press, 612 pp.

Shapiro, M. A., L. S. Fedor, and T. Hampel, 1987: Research aircraft measurements of a polar low over the Norwegian Sea. *Tellus,* **39A,** 272–306, doi:10.1111/j.1600-0870.1987.tb00309.x.

Shkolnik, I. M., and S. V. Efimov, 2013: Cyclonic activity in high latitudes as simulated by a regional atmospheric climate model: Added value and uncertainties. *Environ. Res. Lett.,* **8,** 045007, doi:10.1088/1748-9326/8/4/045007.

Wilhelmsen, K., 1985: Climatological study of gale-producing polar lows near Norway. *Tellus,* **37A,** 451–459, doi:10.1111/j.1600-0870.1985.tb00443.x.

Xia, L., M. Zahn, K. I. Hodges, F. Feser, and H. V. Storch, 2012: A comparison of two identification and tracking methods for polar lows. *Tellus,* **64A,** 17196, doi:10.3402/tellusa.v64i0.17196.

Yanase, W., H. Niino, and K. Saito, 2002: High-resolution numerical simulation of a polar low. *Geophys. Res. Lett.,* **29,** doi:10.1029/2002GL014736.

Zahn, M., and H. von Storch, 2008a: A long-term climatology of North Atlantic polar lows. *Geophys. Res. Lett.,* **35,** L22702, doi:10.1029/2008GL035769.

——, and ——, 2008b: Tracking polar lows in CLM. *Meteor. Z.,* **17,** 445–453, doi:10.1127/0941-2948/2008/0317.

——, and ——, 2010: Decreased frequency of North Atlantic polar lows associated with future climate warming. *Nature,* **467,** 309–312, doi:10.1038/nature09388.

Zappa, G., L. C. Shaffrey, and K. I. Hodges, 2013a: The ability of CMIP5 models to simulate North Atlantic extratropical cyclones. *J. Climate,* **26,** 5379–5396, doi:10.1175/JCLI-D-12-00501.1.

——, ——, ——, P. G. Sansom, and D. B. Stephenson, 2013b: A multimodel assessment of future projections of North Atlantic and European extratropical cyclones in the CMIP5 climate models. *J. Climate,* **26,** 5846–5862, doi:10.1175/JCLI-D-12-00573.1.